JOURNAL OF SPACECRAFT AND ROCKETS
Vol. 47, No. 3, May–June 2010

Experimental Charging Behavior of Orion UltraFlex Array Designs

Joel T. Galofaro,* Boris V. Vayner,† and Grover B. Hillard*
NASA John H. Glenn Research Center at Lewis Field, Cleveland, Ohio, 44135

DOI: 10.2514/1.47285

The present ground-based investigations give the first definitive look, describing the charging behavior of Orion UltraFlex arrays in both the low-Earth-orbital and geosynchronous environments. Note the low-Earth-orbital charging environment also applies to the International Space Station. The geosynchronous charging environment includes the bounding case for all lunar mission environments. The UltraFlex photovoltaic array technology is targeted to become the sole power system for life support and onorbit power for the manned Orion crew exploration vehicle. The purpose of the experimental tests is to gain an understanding of the complex charging behavior to answer some of the basic performance and survivability issues to ascertain if a single UltraFlex array design will be able to cope with the projected worst-case low-Earth-orbital and geosynchronous charging environments. Stage 1 low-Earth-orbital plasma testing revealed that all four arrays successfully passed arc threshold bias tests down to −240 V. Stage 2 geosynchronous electron-gun-charging tests revealed that only the front-side area of indium–tin–oxide-coated array designs successfully passed the arc frequency tests.

Nomenclature

E_B = beam energy, keV
I_c = collected string current, A
I_D = beam current density, nA/cm^2
I_p = string parasitic-current-loss percentage
I_{pv} = string peak current, A
N_e = electron number density, cm^{-3}
T_e = electron temperature, eV
V_B = array bias potential, kV
V_f = floating potential, V
V_{op} = array string operating voltage, V
V_p = plasma potential, V
V_{pv} = string peak voltage, V

I. Introduction

THE Orion's old 28 V and present 120 V UltraFlex arrays represent a unique design challenge [1–5]. The array designs will encounter a number of different space environments, ranging from low-Earth orbital (LEO) to cislunar, with brief passage through the Van Allen belts and the lunar mission environments. Fortunately, all cislunar and lunar mission environments can be effectively categorized under a broader category termed the geosynchronous (GEO) environment case. Thus, there are only two spacecraft environments that apply: LEO and GEO.

Traditionally, photovoltaic arrays are designed for a single environment. For the Orion mission, a single array design is needed for operation in both LEO and GEO space environments. Preliminary risk identification for the crew exploration vehicle (CEV) was made early on by the Orion project team [6]. The Orion team study pointed to four major issues: 1) atomic oxygen (AO) degradation of indium–tin–oxide (ITO) coatings in LEO, 2) electrostatic discharge (ESD) breakdown of dielectric coatings in GEO during geomagnetic substorm events, 3) ESD due to pinholes or damage caused by micrometeorite impacts or orbital debris, and 4) sputtering of ITO coatings and related array contamination.

LEO deployment and operations involve exposure to relatively cold dense plasma with well-known interaction issues: floating potential shifts, parasitic power loss, arcing, and AO sputtering. Parasitic current collection and the resulting associated power losses from the array are closely related to a highly nonlinear phenomenon, termed snapover [6–8]. Surface snapover represents a sudden change from a low current collection regime to a high collection current regime. Under snapover conditions, a small pinhole in a dielectric surface can collect much more current, as if the entire surface of the dielectric were a conductor. Thus, the high-voltage Orion array must be tested against a sudden increase in current collection. The International Space Station's (ISS's) floating potential probe measurements revealed that potential spikes of 40 V negative could present the danger of arcing to an astronaut's space suit [9–11]. The deployment of high-voltage Orion solar arrays in LEO to the ISS also demand reevaluation of floating potential peaks and differential charging on CEV surfaces.

The GEO environment is characterized as relatively low-density plasma with high-energy particles (protons and electrons) subject to violent magnetic storms [6,12]. As a spacecraft passes though the substorm environment, differential charging can reach a few kilovolts, which creates the danger of powerful electrostatic discharge. During its course to cislunar orbital space, the Orion spacecraft will basically see three GEO-space charging environments, spending approximately 73.5% of its time in the solar wind, 13.3% of its time in the Earth's magnetosheath, and about 13.2% of its time in the Earth's magnetotail. Table 1 gives a comparison of the worst-case charging environments [6,12].

The general practice for spacecraft designers has been to use a single spacecraft design for operation in the LEO environment and a separate spacecraft design for operation in the GEO environment. As a result, the common practice of photovoltaic array manufacturers is to force the array cell SiO_2 cover slide to become conducting by overcoating the insulating cover with a thin layer of ITO for operation in the GEO environment. Because a single Orion array design is required for operation in both LEO and GEO environments, the consensus made by the Orion CEV project team was to apply ITO coatings on each of the photovoltaic array surfaces. The Orion arrays are also required to have AR magnesium fluoride (MgF_2) coatings over the ITO layers on each cell. These MgF_2 layers have a thickness of $\sim$0.1 μm, defined by the optical requirements. Ground test results clearly demonstrated that the AR resistivity ($\sim 10^9$ Ω per square) is low enough to bleed off charge in the GEO environment.

Presented as Paper 3525 at the 1st Atmospheric and Space Environments Conference, San Antonio, TX, 22–25 June 2009; received 22 September 2009; revision received 21 January 2010; accepted for publication 29 January 2010.

*Electrical Engineer, Photovoltaic and Space Environments Branch, 21000 Brookpark Road.

†Senior Scientist, Ohio Aerospace Institute, 21000 Brookpark Road, Cleveland, Ohio 44135. Member AIAA.

Table 1 Worst-case GEO charging environments

	Design case	Solar wind	Magnetosheath	Magnetotail
Electron density, cm^{-3}	1.12	9.5	1.1	0.16
Electron temperature, eV	1.2×10^4	12.1	26.9	145.6
Proton density, cm^{-3}	0.24	8.7	1	0.15
Proton temperature, eV	2.95×10^4	10.3	79.9	610.1

The reported tests of the new UltraFlex array designs are the first of their kind, detailing the expected charging behavior under extreme LEO and GEO environments. First and foremost, the purpose of the current experimental research is to ascertain if each of the manufactured array cell types can satisfactorily perform ESD-free under worst-case LEO and GEO charging conditions. Second, the reported research will be used to determine if a single array design can be effectively used for operation in both the LEO and GEO flight regimes, to determine the relative strength and weakness of each of the different manufactured array cells, with the expressed intent of deciding in the very near future which array cell manufacturer will be chosen for integration in the final Orion CEV UltraFlex array design.

II. Experimental Apparatus

Tests were conducted in the Plasma Interaction Facility's (PIF's) Tenney charging-simulator (VF-20) chamber (see Fig. 1 for details). (Vacuum chamber dimensions were 1.8 m diameter by 1.5 m length.) The chamber is equipped with a large 0.9-m-diam cryogenic pump that provides a background pressure of 2×10^{-7} torr. A digital ionization gauge was used to monitor the chamber pressure. The chamber is equipped with a Kaufman-type discharge source that ionizes xenon gas neutrals via a hot filament cathode. The xenon discharge source was used to simulate the electrical charging conditions encountered in the LEO environment. Tank pressure was adjusted by slowly bleeding xenon gas neutrals into the chamber until a pressure of 5.0×10^{-5} torr was achieved with the discharge source operating. Plasma parameters were obtained by sweeping a Langmuir probe (LP) ($N_e = 3.510^6$ cm^{-3} and $T_e = 0.25$ eV). For GEO testing, the vacuum chamber was pumped down to the base tank pressure, and the array assemblies were allowed to outgas in the chamber for a minimum of 8 h before testing. Two electron guns (EGs) with matching 0 to 20 kV power supplies were mounted at the far end of the chamber and pointed at the array. GEO charging was simulated by irradiating the cells-in-circuit (CIC) assemblies with e-beams ($\sim$1 nA/cm^2 current density). A two-dimensional (2-D) positioning system was installed in front of the array. The 2-D positioning system carried an electrostatic noncontact probe for measuring potentials on the surfaces of the array and also included a Faraday cup (FC) for measuring beam-current density. A digital high-impedance voltmeter was used to plot and probe potential distribution via a laptop computer. In principal, only the source-facing side of the array can be tested because of wake effects caused by shadowing of the backward-facing array surfaces. Therefore, the vacuum chamber needs to be reopened and the array flipped for retesting the back-side array surfaces.

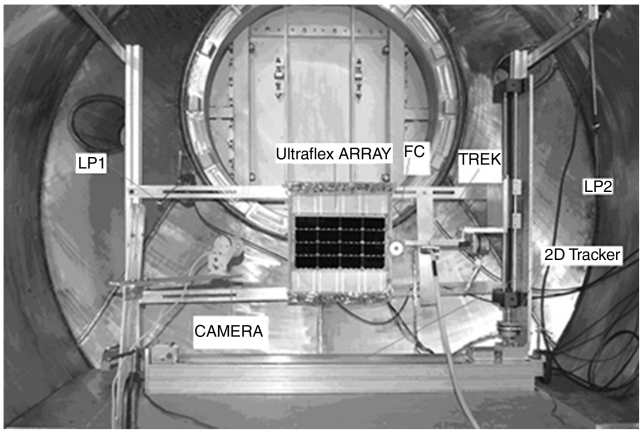

Fig. 1 Snapshot showing Tenney-charging-simulator VF-20 chamber.

Array testing was limited to just four individual development level assemblies: two each from two different cell manufacturers. One array manufacturer provided assemblies with series-z triple-junction monolithic (ZTJM) cell design: one AR-coated (AR–ZTJM) and one with an ITO coating (AR–ITO–ZTJM). The second array manufacturer provided assemblies containing the next generation series of x-triple-junction (XTJ) assemblies: one with an AR coating (AR–XTJ) and one with an ITO coating (AR–ITO–XTJ). Although not included on the CIC's assemblies that were tested, the flight solar array strings incorporated blocking diodes that acted to limit current in the case of sustained arcing between adjacent strings. (The array assemblies that were tested have thinned germanium substrates: thinned from 140- to 100-μm-thick ZTJM and 110-μm-thick XTJ, which were designed to save wing mass.)

The layout of each of the four assemblies was identical: four parallel strings with four CIC assemblies per string, wired in series. An insulating silicone-encapsulated Vectran gore mesh was attached to a rigid insulating composite fiberglass (G-11) frame, with the CICs cemented directly to the Vectran mesh. (Mesh encapsulates were CV2568 for the ZTJM array and CV2566 for the XTJ array.) ZTJM arrays used thin conductive strips for each string output lead. The thin conductive strips were brought out to the edge of the frame and terminated via string termination pads. All conducting strips had a thin insulating layer of Tedlar® covering each conductive strip (see Figs. 2a–2d for details). The XTJ arrays had no conductive strips. The XTJ arrays also had a thin insulating Kapton sheet masking off the noncell areas. The back side of the CICs were primed with silicone adhesive by dabbing small amounts of silicone to promote adhesion but leaving some areas of the conductor exposed. Also, areas between the strings were not grouted on all four array CIC assemblies tested.

Circuitry diagrams for testing against ESD inception in both LEO and GEO environments are shown next. Figure 3a shows a resistor–capacitor (R–C) circuit, current probe (CP), and current probe amplifier, which are used to detect primary arcs on the array. An oscilloscope control program code armed the scope and sets the trigger state to ready. When an arc occurred and exceeded a preprogrammed trigger level, waveform (WF) data were recorded to a specified file on the computer, and the scope was then switched back to an autoready mode, awaiting the next arc event. If an arc occurred between two adjacent array strings, the setup in Fig. 3b would be used to check for sustained arcs. A solar array simulator (SAS) power supply with predetermined voltage and current limits was placed between two adjacent array strings where the primary arc was first detected. A color video camera was mounted inside the vacuum chamber, and a video recorder was used to record arcs. Additionally, a quadrupole mass spectrometer was used to monitor gas species in the chamber.

III. Low-Earth-Orbital and Geosynchronous Environments Test Procedures

The following test plan sequence started on delivery of each solar array sample: photographs of the front and back sides of the array were taken before testing, followed by visual inspections to document any anomalies during shipment. Arrays were then delivered to our cell calibration flash simulator laboratory to make a baseline performance measurement at room temperature before ESD testing. Measurements of short circuit current, open circuit voltage,

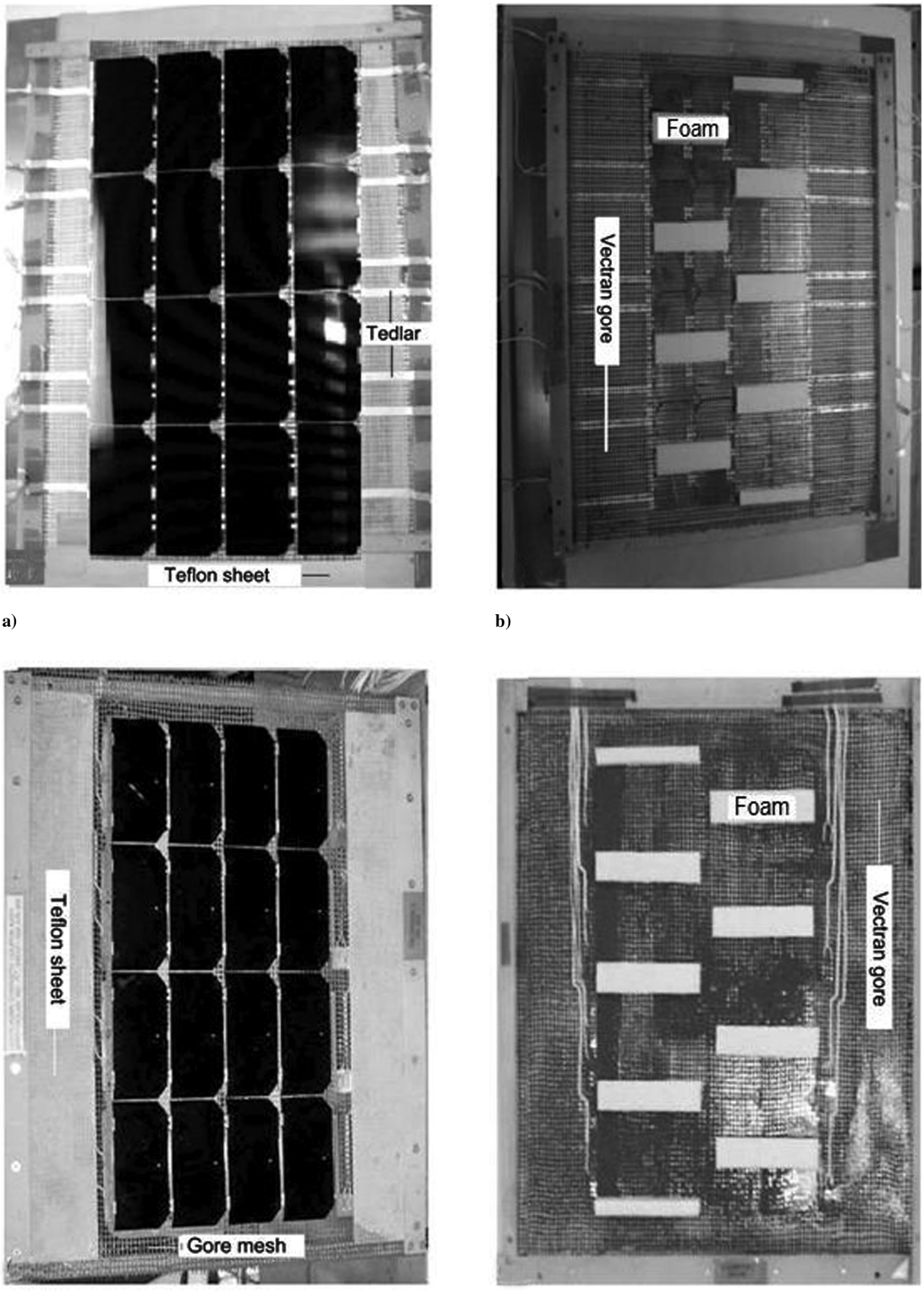

Fig. 2 UltraFlex array: a) front side with AR–ZTJM CICs, b) back side with AR–ZTJM CICs, c) front side with AR–XTJ CICs, and d) back side with AR–XTJ CICs.

maximum voltage, maximum current, maximum power, and cell efficiency were performed on each array string. The array was then delivered to the atomic oxygen facility for a front-side exposure of the AR (or AR/ITO) coatings to measure the performance degradation under AO fluence of $2 \cdot 10^{21}$ atoms/cm^2 and about 8300 equivalent vacuum ultraviolet sun hours. AO and UV exposures were taken simultaneously, and cell efficiency was retested after AO/UV exposure. Photographs were taken to document regions of interest that might be degraded from AO exposure. Photographs indicated some of the Tedlar was eroded after the AO/UV exposure test. Finally, the array was delivered back to the PIF for extensive testing in LEO and GEO environments.

A. Stage 1: Low-Earth-Orbital Test Procedure Details

Figure 1 shows a single ZTJM array mounted in the chamber. The output leads of each array string were shorted together and connected to a separate high-voltage electrical vacuum feedthrough.

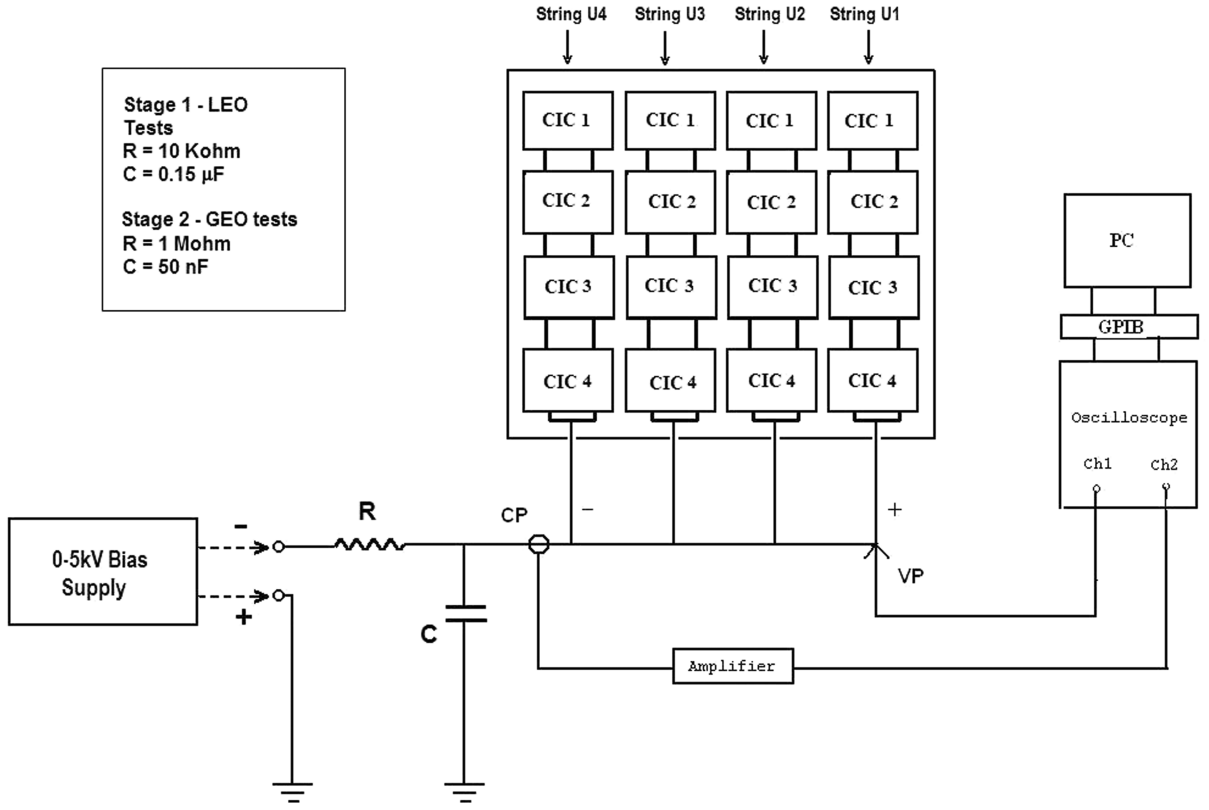

a)

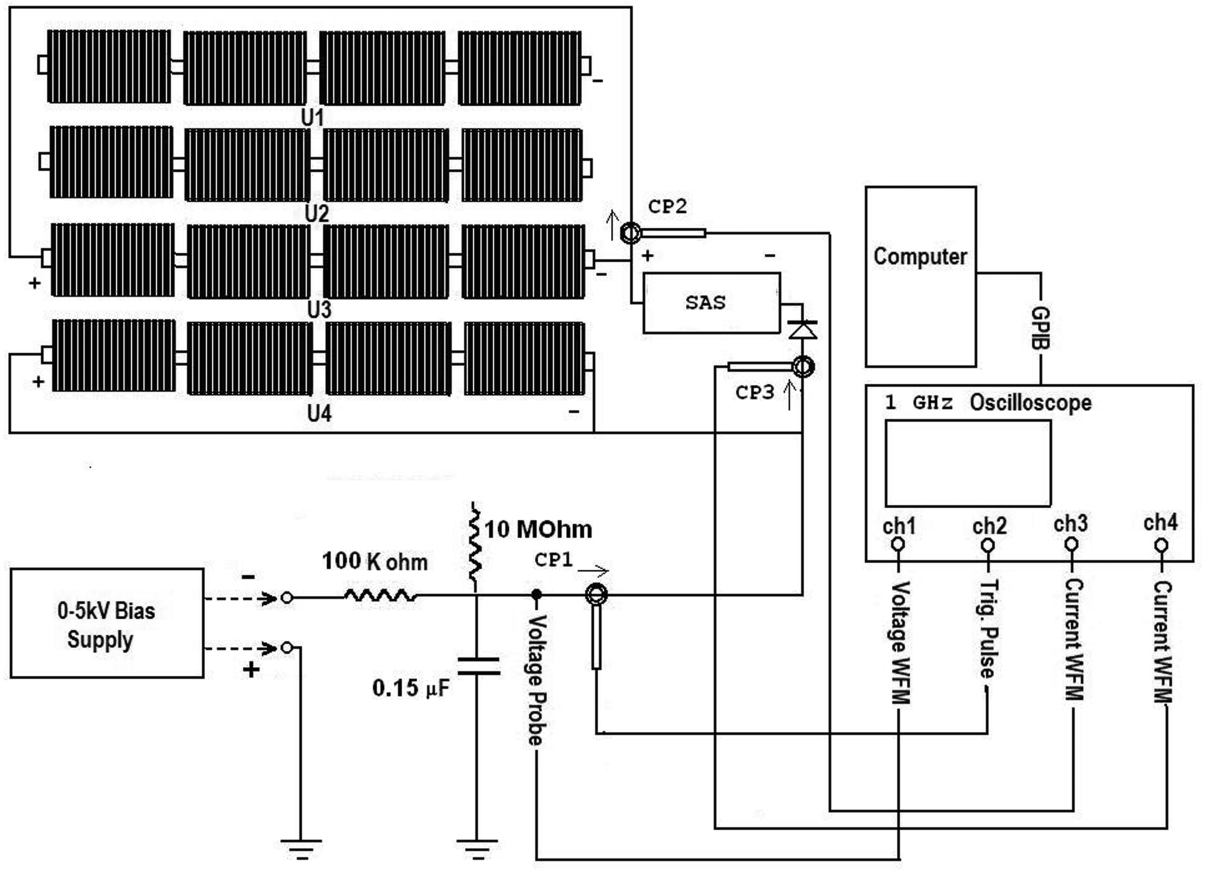

b)

Fig. 3 Circuitry diagrams for testing against ESD inception: a) primary ESD detection circuitry used for LEO arc tests and b) experimental setup used for sustained arc tests. (GPIB denotes general purpose interface bus, R denotes resistor value, C denotes capacitor value, and VP denotes voltage probe.)

Parasitic current for each string was measured separately by sweeping bias voltage within the range of 0 to 120 V. (It is worth noting that the collection current is practically proportional to the number density in our range of interest, because the Debye radius is much shorter than the sample dimension.) The array bias step voltage was held for 1 s before recording the collection current measurement at each voltage step. Finally, estimates for the parasitic losses were obtained, and it was concluded that photovoltaic current losses did not exceeded 0.5%. The parasitic-current-loss estimate applies to the spacecraft's 120 V operating voltage. One example of current-loss calculations for a single string is shown with the floating potential set at both the 90 and 50% operating voltage cases (see Appendix for details).

For the arc threshold tests, the bias voltage was initially set to −40 V and held at this bias level for 60 min. If no arc occurred, the bias voltage was decreased in 10 V decrements, and coupon was retested for another 60 min. The procedure was repeated down to the −120 V bias voltage limit. (The arcing threshold limit of −120 V was modified by the test plan committee after the end of the AR–ITO–ZTJM arc threshold tests. The −120 V limit was replaced by a limit of −240 V as a new margin of safety.) No arc was registered on all four tested samples biased down to 240 V negative. This result negated the necessity of testing against sustained arc inception.

B. Stage 2: Geosynchronous Test Procedure Details

Arcs in GEO environments are generated by differential charging. Differential charging results from a potential difference between the cover glass and the underlying conductor. When an electron beam irradiates the cover-glass surface, its potential goes to the steady-state magnitude. To initiate positive charging of the dielectric, the beam energy needs to be higher than the bias voltage. Therefore, electrons need to strike the cover-glass surface with energy higher than the maximum second electron emission yield (400–600 eV). Crossover energy for most cover-glass ranges between 1.2 to 2 kV. So, in order to initiate positive charging of the dielectric, the beam energy needs to be about 0.6 to 0.8 kV higher than the array bias voltage. However, practical differential charging depends on a combination of array bias voltage, e-beam energy, and secondary electron emission yield [13].

For the stage 2 GEO test procedure, all array strings are shorted together and connected to the negative terminal of a grounded high-voltage power supply. Initially, the array bias V_B is set for −1 kV, and the EG beam energy E_B is set to 1.8 keV, before proceeding. The beam current densities for both EGs are initially set to 1 $\mathrm{nA/cm^2}$, and the array sample is irradiated for 30 min. If an arc occurs during this time span, the array fails to meet the arc frequency criteria. If no arcs are detected at the end of the 30 min irradiation test, the beam-current flux density is increased to 2 $\mathrm{nA/cm^2}$, and the array is allowed to sit under irradiation for another 30 min. All four samples underwent the GEO tests, with current densities of 1, 2, and 5 $\mathrm{nA/cm^2}$ and bias voltages of 1, 2, 3, and 5 kV.

IV. Low-Earth-Orbital and Geosynchronous Test Results

Visual inspections of each array showed no cracks or imperfections to the CIC assemblies, but they pointed out a number of other abnormalities: large exposed conductive strips needed to be insulated, and the Vectran gore mesh needed to be under greater tension to provide a flat surface on which to affix cell assemblies. Slight modifications were made to each array sample at the PIF lab before installation in the VF-20 chamber. These modifications consisted of applications of adhesive-backed Kapton tape to cover up the nonflightlike bus bars and exposed parts of the connecting strips

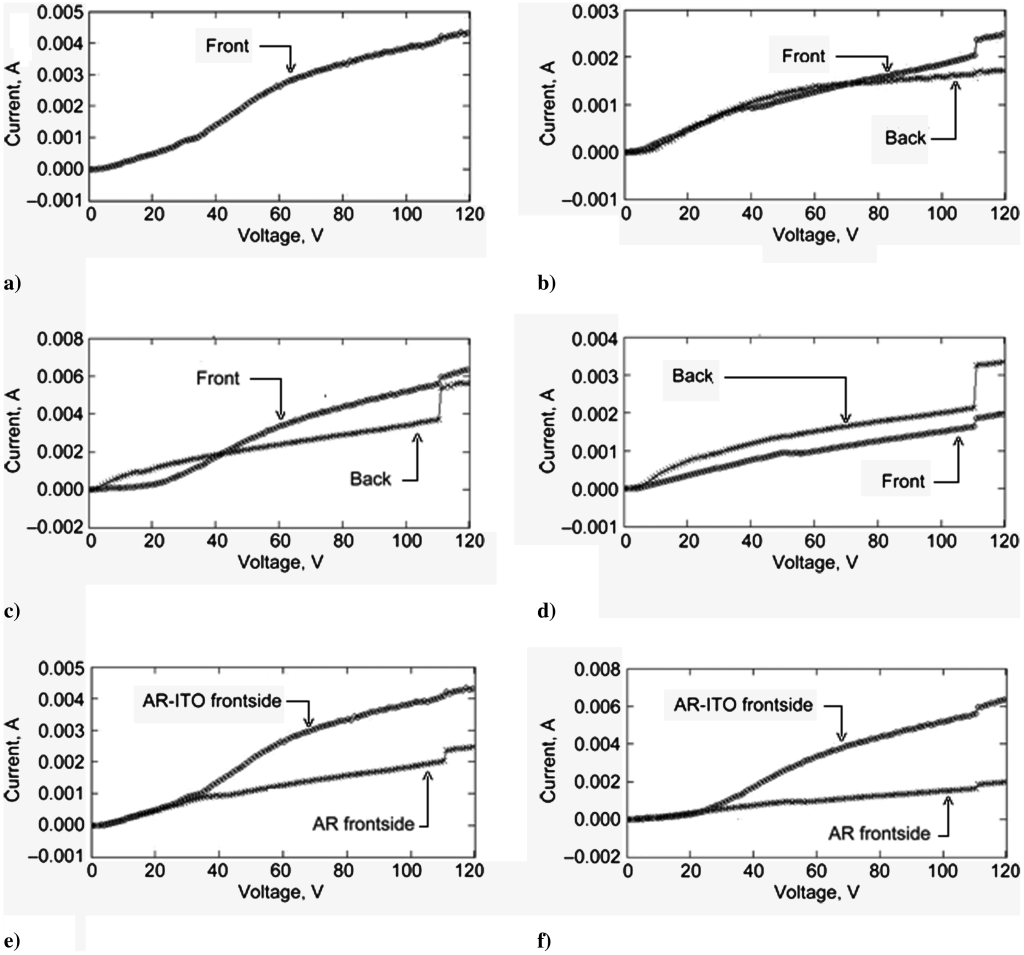

Fig. 4 Current collection for a) front-side AR–ZTJM CICs, b) AR–ZTJM–ITO-coated array CICs, c) AR–XTJ-coated array, d) AR–ITO–XTJ-coated array, e) front-side ZTJM array CICs, and f) front-side XTJ-coated CICs.

in order to decrease errors in the collection current measurements. Kapton tape was also added along the sides of the Vectran gore mesh, not properly affixed to the frame. LEO string current collection was measured by individually biasing each string and sweeping bias voltage between 0 and +120 V in 1 V steps, using a sensitive source meter to record the current at each voltage step. Current collection was measured for the front and back sides of each of the four UltraFlex arrays. Collection current results are plotted for the front side of the AR–ITO–ZTJM CIC sample in Fig. 4a. Front- and back-side current-collection results are plotted for the second AR–ZTJM-coated CICs (see Fig. 4b). Similar plots for the front and back sides of the two AR–ITO–XTJ-coated and AR–XTJ-coated array CICs are shown in Figs. 4c and 4d. Front-side current-collection results are plotted separately for all AR–ITO- and AR-coated array sample assemblies. Current-collection curves are plotted for the AR–ITO–ZTJM in Fig. 4e and for the AR–XTJ array samples in Fig. 4f. The AR–ITO–ZTJM-coated array CICs collected 1.7 to 2 times more current (110 V) than CICs coated only with an AR layer. The current-collection plots (Figs. 4e and 4f) illustrate that the ZTJM-array CICs tend to collect slightly more current than the XTJ array. More quantitative array current-collection results are conveniently summarized in Table 2.

LEO arc threshold tests were performed in separate consecutive 1 h runs, with decreasing negative array bias voltages (−10 V steps) down to the maximum level of 240 V negative. Because there were no primary arcs detected during any of the LEO arc threshold tests, no tests were needed to check against the possibility of sustained arcs. Final LEO arcing threshold test results are shown in Table 3.

A. Geosynchronous Results: Antireflection/Indium-Tin-Oxide/ Z-Triple-Junction-Monolithic Coated Array

All four array strings were shorted together and connected to a high-voltage power supply through the R–C circuit, shown in Fig. 3a (resistor and capacitance values in the R–C circuit were $R = 1$ MΩ and $C = 50$ nF). A problem developed early on in the tests. A number of arcs were registered on the nonflightlike areas on the front of the development level array assembly, even at the lowest levels of charging. Discharges were registered less than 1 min after starting array sample irradiation. Peak current reached 8 A, with a pulse width of about 10 μs (Fig. 5). An electrostatic probe scan of the cell surfaces showed no signs of differential charging; thus, the ITO layer was effectively bleeding off charges. The sample was reirradiated by energizing the EG using the same array bias potential, beam energy, and current density settings, and ten more discharges were generated.

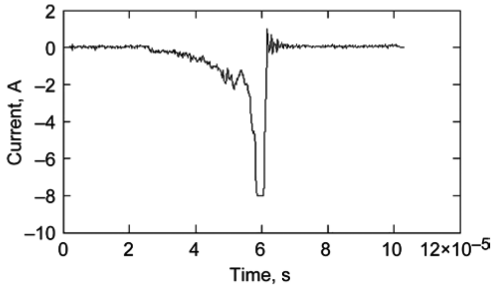

Fig. 5 Example of arc pulse on dielectric Tedlar-covering conducting strip. Charging due to e-beam exposure at low beam energy of 1.1 keV and beam-current density of 1 nA/cm^2.

Arc sites were clearly located: arcs occurred on the exposed thin Teflon-paper sheet and on the Tedlar dielectric coatings. At this point, the decision was made to modify the array by covering all exposed Tedlar strips on the front of the array with Kapton tape (Fig. 6). No modifications were made to the back side of the array. These modifications only allowed testing of the CIC area on the array sample. Even with the Kapton modifications implemented on the ZTJM array, the arcs still struck on the nonflightlike array area (see Fig. 7 for details).

No surface charging was found at current densities of 1, 2, and 5 nA/cm^2 and at beam energy up to 3.5 keV. The array was next biased at −2.9 kV and irradiated with electron-beam energy of 3.5 keV and current density of 7 nA/cm^2. Kapton tape strips were charged, and an arc discharge occurred on the Kapton-covered Tedlar strip (Fig. 7). The sample was dismounted from the VF-20 chamber and brought to the calibration laboratory. There was no indication of visual damage or burn marks on the sample. The calibration laboratory recorded a loss of efficiency in each of the four strings. After the sample was returned, a last attempt was made at biasing the array sample at −2.9 kV and irradiating the sample with a beam energy of 3.5 keV and a beam current density of 7 nA/cm^2 for a 5 min exposure. EG power supplies were shut down, and an electrostatic probe scan was performed directly after e-beam exposure. The horizontal distance between the points was 2.2 mm in Figs. 8a and 8b. The electrostatic probe scan clearly demonstrated charging of the Kapton tape and a complete absence of charging on any of the CIC array surfaces whatsoever (Fig. 8). The AR–ITO–ZTJM array coupon successively passed all stage 2 GEO tests. GEO tests were not performed on the back side of the AR–ITO–ZTJM array.

Table 2 Summary of collected current results scaled to flight conditions for an Orion 28 V power system

Coupon	Current collected at 10 V (25% of max string V_{op} of 35 V), A	Equivalent 19-cell string level current collection, A	Successful test?	Comments
AR–ZTJM	0.00030 front	0.00018	Success	Higher collected current than AR–ITO coupon. Collected current difference increases to a factor 2x at 50 V bias.
AR–ITO–ZTJM	0.00025 front + 0.00016 back = 0.00041 total	0.00026	Success	——
AR–XTJ	0.00020 front + 0.00030 back = 0.00050 total	0.00030	Success	——
AR–ITO–XTJ	0.00020 front + 0.00075 back = 0.00095 total	0.00059	Success	Current collected is above 0.00040 A goal but still acceptably small value of 0.15% of string operating current.

Table 3 LEO arc threshold test results

Coupon	Arc at most negative bias required (−80 V, driven by mated-ISS case)? Yes/No	Arc at most negative bias tested? Yes/No	Successful test?	Comments
AR–ZTJM	No	No (to −120 V)	Success	Good margin demonstrated
AR–ITO–ZTJM	No	No (to −240 V)	Success	Very good margin demonstrated
AR– XTJ	No	No (to −240 V)	Success	Very good margin demonstrated
AR–ITO–XTJ	No	No (to −240 V)	Success	Very good margin demonstrated

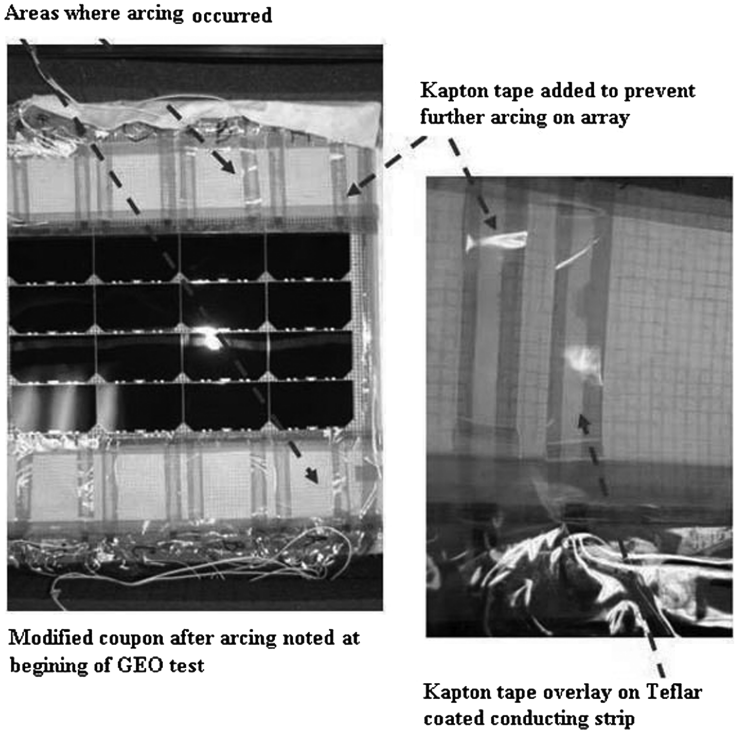

Fig. 6 Modifications made to the ZTJM and XTJ (AR and AR–ITO) UltraFlex array samples.

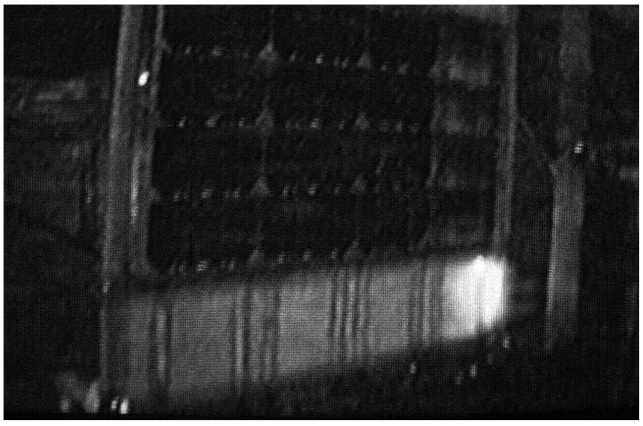

Fig. 7 Snapshot of arc on Tedlar strip triggered with array bias at −2.9 KV, beam energy of 3.5 keV, and EG current density of 7 nA/cm^2.

B. Geosynchronous Results: Antireflection/Z-Triple-Junction-Monolithic Coated Array

Initially, the Emcore AR array was biased at −1.1 kV. Note that the top cell (CIC 1) on the array string U4 was cracked while trying to remove a section of Kapton tape that fell on the cell (see Fig. 3). Figure 9a shows an example of a surface probe scan of potentials for the AR–ZTJM array, biased at 1.1 kV but not irradiated. Figure 9b shows a surface scan of potentials after irradiation, with the array still biased at −1.1 kV under an e-beam using a beam energy of 1.8 keV with a beam current density of 2 nA/cm^2. No arcs were detected, but a scan of surface potentials shows the Emcore AR-coated array appears to have acquired differential charging of CIC on the order of +900 V, which clearly indicates that no ITO layer is present on the CIC assemblies. Beam-current density was increased to 5 nA/cm^2, and one arc occurred on the cracked cell. String U4 was removed from the circuit. Continued irradiation at the previous beam-current density showed no arcing had occurred. The array bias level was increased to −2 kV, with the beam energy raised to 2.8 keV, and the sample was tested at beam-current densities of 1, 2, 5, and 10 nA/cm^2, with no arcs detected on the flightlike cell surfaces. However, three arcs were triggered on the nonflightlike array (the first two arcs occurred on the Teflon sheet, and the third arc was detected on the Kapton-covered Tedlar strip). Resumed testing with the array biased at −3 kV, with beam energy of 3.5 keV and a beam-current density of 2, 3, and 5 nA/cm^2 showed no arcs detected on the flightlike areas of the AR–ZTJM array. Beam-current density was increased to 10 nA/cm^2, and a discharge occurred in the area covered by Kapton tape after 10 min of irradiation (Fig. 10). Note that

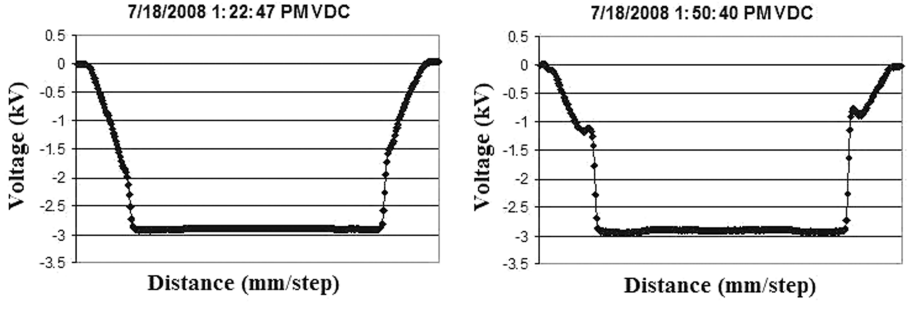

a) b)

Fig. 8 Electrostatic a) probe surface scan with array biased at −3 kV but not irradiated and b) surface potential scan after 5 min irradiation, with $V_B = -3$ kV, $E_B = 3.5$ keV, and $I_B = 7$ nA/cm^2. (VDC denotes volts direct current.)

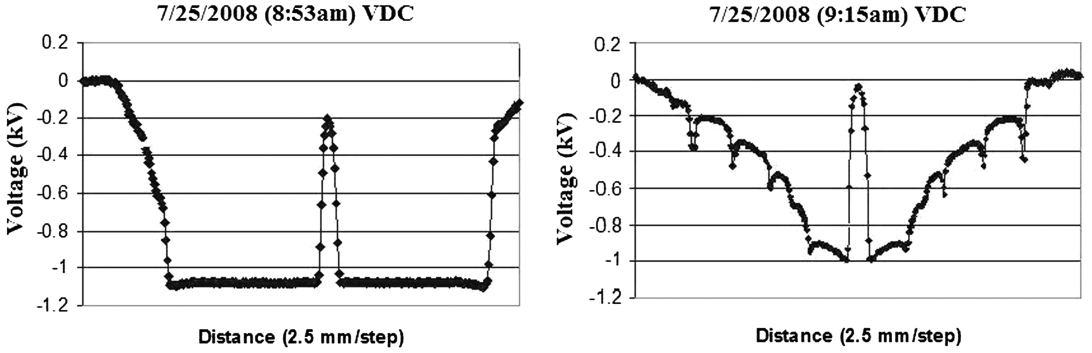

a) b)

Fig. 9 Surface probe scan: a) AR–ZTJM coupon indicated a potential of −1.1 (±0.05) kV before irradiation and b) differential potential of about 900 V after irradiation.

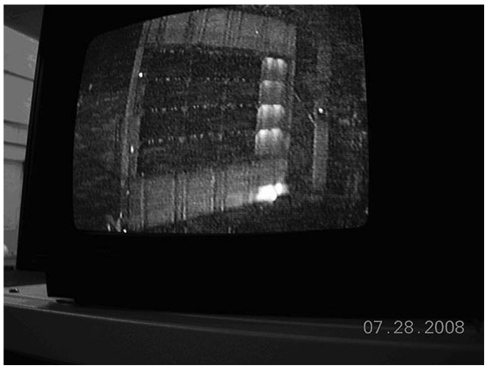

Fig. 10 Discharge on Teflon at −2 kV bias voltage with beam energy at 2.8 keV, with a beam-current density of 10 nA/cm^2.

Fig. 11 Snapshot of AR–ZTJM-coated array showing multiple discharges under bias at −9.5 kV and irradiated with 10 keV beam energy and 5 nA/cm^2 beam-current density.

four lighted CICs above the arc site in Fig. 10 appear to be due to current flowing through the array string CICs.

The chamber was opened, and additional Kapton covers were added to areas of the composite frame and connecting strips. The array sample bias was increased to −3 kV and irradiated with a beam energy of 3.5 keV with a current density of 2 nA/cm^2. The first arc occurred on the string U2 interconnect between CICs 3 and 4. A probe scan of surface potentials indicated differential charging up to 1.5 kV. Beam-current density was increased to 3 nA/cm^2, and another arc occurred on the interconnect between CICs 3 and 4 on string U1. Beam current was increased to 5 nA/cm^2, and an arc occurred between cell 3 on string U1 and cell 3 on string U2. A final arc was detected about 15 min later on string U3 between CICs 2 and 3. Therefore, the front side of the AR-coated ZTJM array failed to pass stage 2 GEO tests due to arcing on the flightlike areas of the array.

The chamber was opened, and the ZTJM array was reinstalled with the EGs pointed directly at the back side of the array. Back-side testing started the −2 kV array bias. No arcs were detected in a 17 min test, under irradiation with beam energy of 2.8 keV and beam-current density of 5 nA/cm^2. Bias level of the array was increased to −3 kV, with beam energy set to 3.5 keV and a beam-current density of 1 nA/cm^2. One arc occurred near the top-left side of the Kapton cover. Two more arcs were detected on the back side of the array, in the area on the conducting strip near the edge of the composite frame. Array bias voltage was increased to −5 kV, and the back side of the array was irradiated with e-beam energies of 5.7 keV, with a current density of 5 nA/cm^2. Three more arcs were recorded: one arc occurred near the top-middle region of the array on the Kapton cover, applied over the composite frame, and the other two arcs occurred on the Vectran gore mesh near the string-conducting strips. A final attempt was made to see the effects of charging the back side of the array at extreme GEO levels, well beyond those expected during flight. For this test, the array sample was biased at 9.5 kV, and the back side of the array was irradiated with a beam energy of 10 keV and a current density of 10 nA/cm^2. This extreme charging test

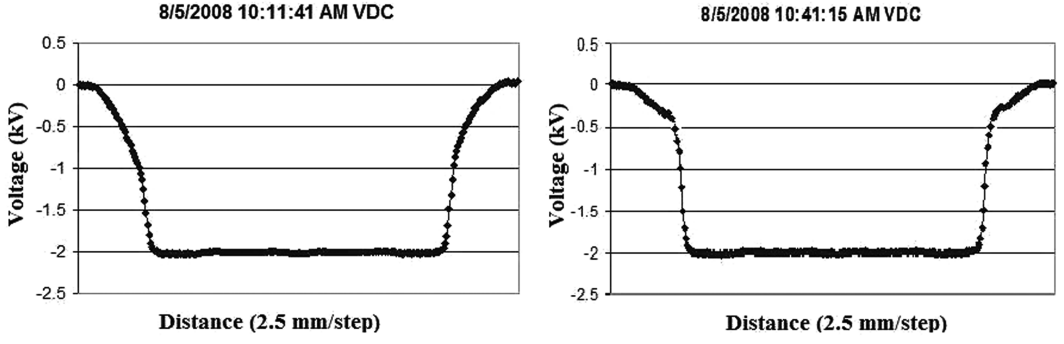

a) b)

Fig. 12 Surface potential scan a) array biased at −2 kV and b) after irradiating biased array with e-beam energy of 2.5 keV and beam flux of 2 nA/cm^2.

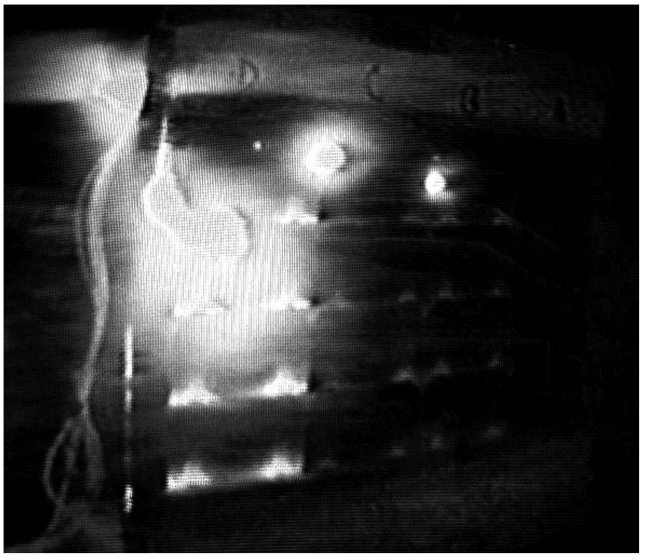

Fig. 13 Multiple discharges at bias potential −5 kV, beam energy 5.5 keV, and beam-current flux of 5 nA/cm^2. Discharges are located on the cable leads.

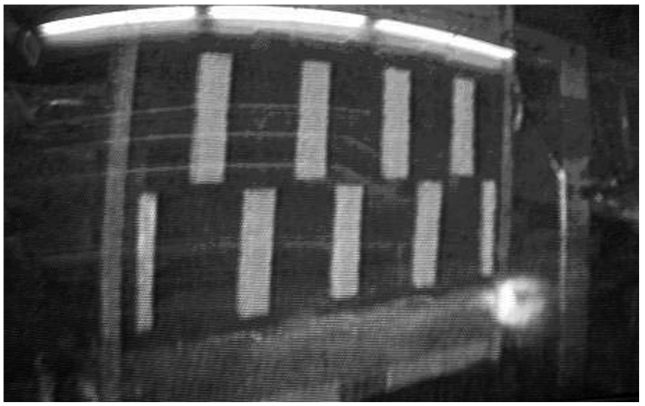

Fig. 14 Arc discharge on back side of the AR–ITO–XTJ-coated array. Arc initiated at −2 kV bias and irradiated at 2.5 keV energy, using a 5 nA/cm^2 current flux.

resulted in a multiple number of very intensive arc discharges scattered over the face of the back side of the array (Fig. 11).

C. Geosynchronous Results: Antireflection/Indium-Tin-Oxide/X-Triple-Junction Coated Array

All four strings were biased at a −2 kV potential, and a Trek probe scanned across the surface of the array. The array surface was next

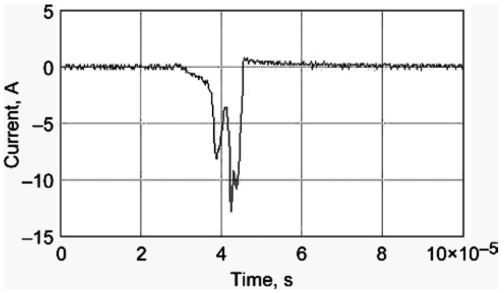

Fig. 16 Current pulse registered at −3 kV bias, beam energy of 3.6 keV, and current flux of 5 nA/cm^2.

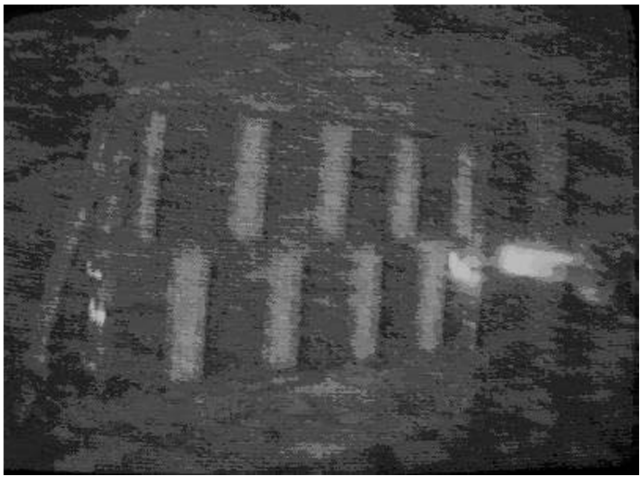

Fig. 17 An arc discharge on back side of AR–XTJ-coated array. Discharge recorded using bias at −3 kV under e-beam irradiation energy of 3.6 keV and current flux of 2 nA/cm^2.

irradiated with e-beam energy of 2.5 keV, with an e-beam current flux of 2 nA/cm^2. No arcs occurred in the 20 min allotted-time interval. A surface potential scan demonstrated that the ITO layer effectively prevented differential charging (Fig. 12). Beam-current density was increased to 5 nA/cm^2, and no arcing occurred at the −2 kV bias level. Bias voltage was then increased to −3 kV, exposed to e-beam, and irradiated for 15 min, with beam energy at 3.5 keV and an e-beam flux of 5 nA/cm^2. One arc occurred at the dielectric and conductor junction, located at the bottom-right corner on the bus bar. Continued irradiation of the sample for another 15 min, using the same beam parameters, showed that no arcs occurred, and an electrostatic probe scan demonstrated the absence of the differential charging of array surfaces. Finally, the array bias and beam energy were increased to −5 kV and 5.5 keV, respectively, using a current beam flux of

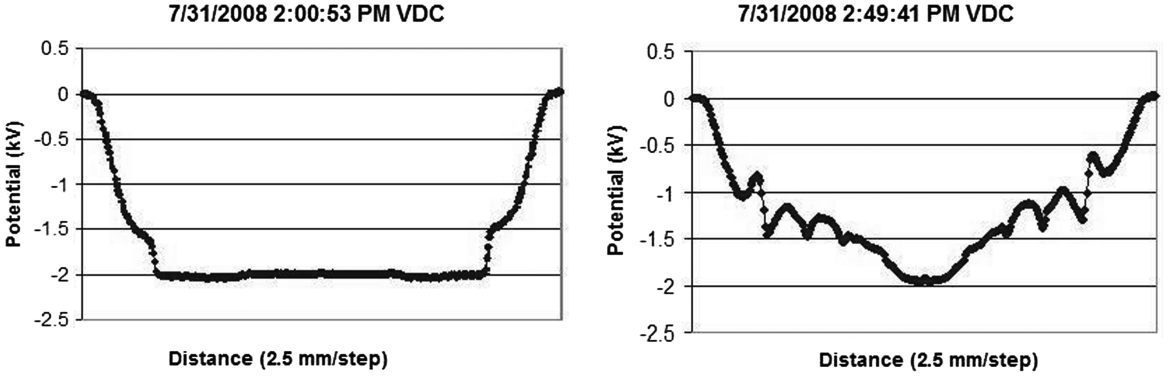

a) b)

Fig. 15 Surface potential scan: a) array biased at −2 kV and b) after 10 min of irradiation with beam energy of 2.8 keV and beam flux of 3 nA/cm^2.

Table 4 Summary of stage 2 GEO tests for front side and back side of all four ZTJM and XTJ UltraFlex array sample assemblies

CICs	Arcing at or below most negative bias and e-beam charging parameter tested? Yes/No	Any arcing margin? Yes/No	Successful test?	Comments
		ZTJM–AR–ITO		
Front to e-beam	No (up to −3 kV, 3.5 keV, 7 nA/cm^2, 0 V differential charging)	Not tested	Successful[a]	CICs with ITO on the cover show a complete lack of differential charging under e-beam exposure, as confirmed by electrostatic probe data. Arcing occurred on nonflight array cabling at −1.1 kV bias, 2 keV energy, and 1 nA/cm^2 flux, ∼10 A. Arcs caused degraded IV performance of array.
Back to e-beam	Not tested	Not tested	Not tested	——
		ZTJM–AR		
Front to e-beam	Yes (at −3 kV, 3.5 keV, 2 nA/cm^2, 1.5 kV differential)	No	Unsuccessful	CICs without ITO on the cover glass are subjected to large differential charging under e-beam exposure. Arcing occurred on nonflight cabling at −1.1 kV bias, 2.8 keV energy, and 5 nA/cm^2 flux. 10 A arcs degraded array IV performance.
Back to e-beam	No (up to −5 kV, 5.7 keV, 5 nA/cm^2)	Yes (arcs at next test point of −9.5 kV, 10 keV, 5 nA/cm^2	Successful	——
		XTJ–AR		
Front to e-beam	Yes (−2 kV, 2.8 keV, 1 nA/cm^2, 0.8 kV differential)	N/A, not tested	Unsuccessful	Coupon arced at string termination point on round wire cable. CICs arced at −2 kV, 2.8 keV energy and 5 nA/cm^2 flux. Differential bias 1.3 kV.
Back to e-beam	Yes (−3 kV, 3.6 keV, 2 nA/cm^2)	N/A, not tested	Unsuccessful	——
		XTJ–AR–ITO		
Front to e-beam	No (up to −5 kV, 5.5 keV, 5 nA/cm^2, 0 V differential)	N/A, not tested	Successful[b]	Coupon arced at string termination pad and at the connection point with the round wire cable. Array bias −3 kV under e-beam exposure. 3.5 keV energy and beam 2 nA/cm^2.
Back to e-beam	Yes (2 kV, 2.5 keV, 5 nA/cm^2)	N/A, not tested	Unsuccessful	——

[a]CICs not tested to full charging conditions; coupons arced at nonflightlike cabling.
[b]CICs readily arced at nonflightlike string termination pad at round wire connection.

2 nA/cm^2. No arcs were found during the 15 min exposure time. Increasing the current flux to 5 nA/cm^2 resulted in multiple discharges, which appeared to originate at the dielectric and conductor junctions located at the top of the array in Fig. 13. Continued sample irradiation occurred for an additional 17 min at the same bias at the −5 kV level, with beam energy of 5.5 keV and the current flux set to 5 nA/cm^2, with no arcs being registered. An extended 1 h test of the sample, with the same parameters, resulted in five arcs being registered, all occurring on the nonflightlike dielectric and conductor junctions, located at the bottom of the array. The front-side flightlike array segments of the AR–ITO–XTJ array successfully passed the stage 2 GEO tests. The ITO layer bleeds charge perfectly, but arcing appears to result from adjacent dielectric (Kapton) and conductor (ITO) junctions.

The chamber was opened, and the array was mounted with the back side facing the EGs. When testing resumed, the back side of the array was biased at −2 kV and irradiated at beam energy of 2.5 keV and beam current flux of 5 nA/cm^2 in a 30 min test. Four arcs were registered on back of the array. The bias level was then increased to −3 kV and irradiated with a 3.5 keV beam, having a beam-current flux of 5 nA/cm^2, which resulted in four more arc discharges being registered. One example of an arc on the back side of the array is shown in Fig. 14. As a result, the back side of the Spectrolab AR–ITO–XTJ array failed to pass the stage 2 GEO tests.

D. Antireflection Geosynchronous Results: Antireflection/X-Triple-Junction Coated Array

Output leads of all the four strings of the AR–XTJ array were connected to the negative terminal of the high-voltage power supply through the R–C network (Fig. 3). All four array strings were biased at −2 kV, and a surface potential scan was performed before irradiating the array assemblies (Fig. 15a). The array was then irradiated with 2.8 keV and a 1 nA/cm^2 beam. The first arc occurred on the top-right corner of array string U1, and a second arc occurred at the same site after 2 min of irradiation. A third arc was recorded at the same position as the first two arcs, some 7 min later. Beam current was increased to 3 nA/cm^2. One arc was registered on the bus bar, at the top of string U3. After a total of 10 min under irradiation, an electrostatic probe scan indicated differential charging of approximately 800 V (Fig. 15b).

One arc occurred at the top-right corner of the array. The e-beam flux was increased to 5 nA/cm^2, and a second arc was triggered at the same location. The vacuum chamber was opened, and both bus bars were covered with Kapton tape. The sample was reinstalled in the chamber and allowed to pump down to the base operating pressure. Testing resumed by biasing the array at −2 kV and irradiating it with a beam energy of 2.8 keV and an e-beam current flux of 5 nA/cm^2. An arc discharge was initiated between CICs 1 and 2 on string U1, after 7 min under irradiation. The bias voltage, beam energy, and current flux were increased to −3 kV, 3.6 keV, and 2 nA/cm^2, and another arc was registered at the same location (top-right corner of string U1) after 3 min of e-beam exposure. Increasing the e-beam current flux to 5 nA/cm^2 resulted in four more arcs. Figure 16 shows a plot of the current pulse recorded for the fourth arc discharge. As a result, the front side of the AR–XTJ-coated array failed to pass the stage 2 GEO tests.

The chamber was opened, and the AR–XTJ-coated array was pointed, with the back side of the array facing the two EGs. Arc discharges began to be registered at a bias voltage set to −3 kV and when subsequently exposed to e-beam irradiation, using beam energy of 3.6 keV and a current density of 2 nA/cm^2. A snapshot taken from the video record of an arc discharge on the back side of the array is shown in Fig. 17. Beam-current flux was next increased (5 nA/cm^2) at the same beam energy and array bias potential. Another arc discharge was initiated on the back side of the array. As a result, the back side of the AR–XTJ array sample also failed to pass stage 2 GEO tests. A summary of the front- and back-sides stage 2 GEO tests results for all ZTJM and XTJ arrays tested is given in Table 4.

V. Conclusions

Generally speaking, all ZTJM and XTJ UltraFlex (AR- and AR–ITO-coated) development-level array coupon designs successfully passed the stage 1 LEO tests results, showing no signs of arcing at an ambient test temperature down to −240 V array bias. The AR- and AR–ITO-coated ZTJM and XTJ CICs and the interconnect regions appeared to be well designed for operating ESD-free in an LEO plasma environment. Furthermore, the reported current-collection measurements are low (∼4 mA), even for the AR–ITO–XTJ-coated array sample, which collects slightly more current than the ZTJM array; thus, parasitic current loss should not be an issue for either of these arrays, as part of an Orion 120 V power system. The front side of the ITO-coated CIC samples from the ZTJM and XTJ arrays also appears to be suitable for use in the GEO charging environments, because the ITO-coated array CICs did not arc on the front-side flightlike regions of the array. (Surface potential scans after e-beam irradiation show that the ITO layer effectively bleeds off the charge.) ZTJM and XTJ CIC assemblies layered with ITO are extremely promising in mitigating differential charging effects on the front side of the array, but they require some flight design refinements in order to improve the safety of operations in the GEO and lunar mission environments. For example, minor design changes are needed to eliminate differential charging effects on the Teflon mask and the Tedlar dielectric coatings. String termination pads and wiring need to be redesigned to eliminate arcs in the respective regions of the array. The back side of the array CICs needs to have a controlled minimal amount of silicone insulation in order to prevent arcing in the GEO environment. Arcing occurred at nonflightlike heavy continuous-mesh-adhesive regions that allowed for high charging potential when compared with the same adhesive on the sparse mesh over the solar-cell back sides. The coupon back-side-material GEO-charge surface potential scan data showed this behavior. The current test results have provided much valuable information concerning the expected complex charging behavior and survivability of the Orion CEV UltraFlex array design in both the LEO and GEO mission environments. Future tests are planned to explore coupon arcing characteristics over a wider range of operating temperatures and bias voltages. Also, plasma interaction testing, with higher fidelity Orion UtraFlex solar array assemblies, are planned for the future. In conclusion, a single UltraFlex photovoltaic array can be designed to satisfactorily cope with extended operations in LEO and GEO environments, provided design refinements are implemented to improve robustness against arcing.

Appendix: Example Calculation of Parasitic Current Loss for a Single String

Parasitic current loss I_c for a single string is compared against photovoltaic current loss Ip and is expressed as a simple ratio I_c/I_{pv}. The string operating voltage $V_{\text{op}} = 120$ V and the floating potential V_f are assumed to be 90% of the string operating voltage, $V_f =$ 120 V. The positive voltage peak $V_{\text{pv}} = (V_{\text{op}} - V_f)$ or $V_p = 12$ V potential. A collected current plot versus voltage (from actual data) is given for the Spectrolab XTJ–AR array string U1, shown in Fig. A1.

The collected string current I_c is integrated over the entire plot at a positive voltage peak value, $V_{\text{pv}} = (V_{\text{op}} - V_f) = 12$ V. I_c is calculated from

$$I_c = \frac{1}{V_{\text{pv}}} \int_{i=0}^{v_{\text{pv}}} I(v)\ \mathrm{d}v = \frac{1}{12} \sum_{k=1}^{12} I_i(v_i) \tag{A1}$$

Therefore, the collected current value yields: $I_c = 7.1 \times 10^{-5}$ A

Assuming the peak current I_{pv} from a single string is $I_{\text{pv}} = 0.5$ A, then I_p gives the gives the required ratio for calculating the magnitude of the parasitic current loss of string U1 in Eq. (A2):

$$I_p = \frac{I_c}{I_{\text{pv}}} = \frac{7.1 \times 10^{-5}}{0.5} = 1.1 \cdot 10^{-3} = 0.00014\ \% \tag{A2}$$

If the floating potential V_f is now assumed to be 50% of the operating potential, $V_{\text{op}} = 120$ V, then $V_f = (0.5)(120) = 60$ V, and the

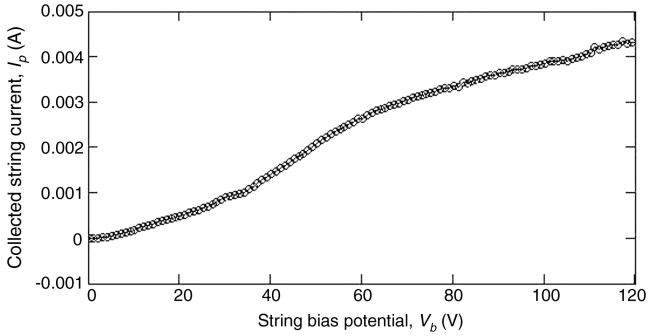

Fig. A1 Collected current plate for AR–XJT string U1.

positive peak voltage is $V_{\text{pv}} = (120 - 60) = 60$ V. The collected current I_c computed from the curve is then specified in Eq. (A3):

$$I_c = \frac{1}{V_{\text{pv}}} \int_{i=0}^{v_{\text{pv}}} I(v)\ \mathrm{d}v = \frac{1}{60} \sum_{k=1}^{60} I_i(v_i) \tag{A3}$$

The value of the collected current I_c now becomes

$$I_c = 5.5 \cdot 10^{-4}\ \text{A}$$

The parasitic current loss I_p from string U1 can then be similarly computed from the ratio in Eq. (A4):

$$I_p = \frac{I_c}{I_{\text{pv}}} = \frac{5.5 \times 10^{-4}}{0.5} = 1.1 \cdot 10^{-3} = 0.11\% \tag{A4}$$

Acknowledgments

The authors wish to express their gratitude to the following companies for supplying the needed cells-in-circuit (CIC) assemblies and technical specifications for these experiments: Lockheed–Martin Corporation [prime contractor for integration of UltraFlex arrays on crew exploration vehicle (CEV)], ATK Space Systems in Goleta, CA (subcontractor for design/fabrication of Orion UltraFlex arrays on CEV), Emcore Corporation (z-triple-junction-monolithic CIC manufacturer), and Spectrolab, a subsidiary of Boeing (x-triple-junction CIC manufacturer).

References

[1] White, S., Douglas, M., Spence, B., Jones, P. A., and Piszczor, M. F., "Development of an UltraFlex-Based Thin Film Solar Array for Space Applications," *2003 Proceedings of 3rd World Conference on Photovoltaic Energy Conversion*, Vol. 1, IEEE Publ., Piscataway, NJ, May 2003, pp. 793–796.

[2] Spence, B., White, S., Wilder, N., Gregory, T., Douglas, M., Takeda, R., Mardesich, N., Peterson, H., Sharps, P., and Fatemi, N., "Next Generation UltraFlex Solar Array for NASA's New Millennium Program Space Technology 8 (ST8)," *31st IEEE Photovoltaic Specialists Conference*, IEEE Publ., Piscataway, NJ, Jan. 2005, pp. 826–829.

[3] Sharps, P., Aiken, D., Stan, M., Cornfeld, A., Newman, F., Endicter, S., Hills, J., Girard, G., Doman, J., Turner, M., Sandoval, A., and Fatemi, N., "Space Solar Cell Research and Development Projects At Emcore Photovoltaics," *19th Space Photovoltaic Research and Technology Conference*, NASA CP-2007-214494, pp. 145–152, 2007.

[4] Fetzer, C. M., King, R. R., Law, D. C., Edmondson, T., Isshiki, M., Haddad, J. C., Boisvert, J. C., Zhang, X., Joslin, D. E., and Karam, N. H., "Multijunction Solar Cell Development and Production At Spectrolab," *19th Space Photovoltaic Research and Technology Conference*, NASA CP-2007-214494, pp. 153–159, 2007.

[5] Spence, B., White, S., Jones, A., Wachholz, J., Wilder, N., Cronin, P., Gregory, T., Barker, P., Allmandinger, T., Mardesich, N., Piszczor, M., Sharps, P., and Fatemi, N., "UltraFlex-175 Solar Array Technology Maturation Achievements for NASA's New Millennium Program (NMP) Space Technology 8 (ST8)," *Conference Record of the 2006 IEEE 4th World Conference on Photovoltaic Energy Conversion*, Vol. 2, IEEE Publ., Piscataway, NJ, May 2006, pp. 1946–1950.

[6] Hillard, G., Vayner, B., Galofaro, J., Snyder, D., Dever, J. A., and Miller, S. K., "Preliminary Assessment of Environmental Interactions for the Orion Solar Arrays," NASA TM-2009-215823 (to be published).

[7] Ferguson, D., Hillard, G., Snyder, D., and Grier, N., "The Inception of Snapover on Solar Arrays: A Visualization Technique," AIAA Paper 98-1045, Jan. 1998.

[8] Galofaro, J., Vayner V., Degroot W., Ferguson, D., Thomson, C. D., Dennison, J. R., and Davies, R. E., "Inception of Snapover and Gas Induced Glow Discharges," NASA TM-2000-209645, Jan. 2000, pp. 1–8.

[9] Craven, P., Wright, K., Minow, J., Coffey, V., Schneider, T., Vaughn, J., Ferguson, D. C., and Parker, L. N., "Survey of International Space Station Charging Events," AIAA Paper 2009-0119, Jan. 2009.

[10] Carruth, M. R., Schneider, T., McCollum, M., Finckenor, M., Suggs, R., Ferguson, D., Katz, I., Mikatarian, R., Alred, J., and Pankop, C, "ISS and Space Environment Interactions Without Operating Plasma Contactor," AIAA Paper 2001-0401, Jan. 2001.

[11] Schneider, T. A., Carruth, M. R., Jr., and Hansen, H. J., "Minimum Arc Threshold Voltage Experiments on Extravehicular Mobility Unit Samples," AIAA Paper 2002-1040, Jan. 2002.

[12] Purvis, C. K., Garett, H. B., and Stevens, J. N., "Design Guidelines for Assessing and Controlling Spacecraft Charging Effects," NASA TM 2361, 1984, pp. 1–46.

[13] Vayner, B. V., Ferguson, D. C., and Galofaro, J. T., "Comparative Analysis of Arcing in LEO and GEO Simulated Environments," AIAA Paper 2007-93, Jan. 2007.

I. Boyd
Associate Editor